annalen der **physik**

Transport and dephasing in a quantum dot: Multiply connected graph model

Maximilian Treiber*, Oleg Yevtushenko, and Jan von Delft

Dedicated to Ulrich Eckern on the occasion of his 60th birthday.

Using the theory of diffusion in graphs, we propose a model to study mesoscopic transport through a diffusive quantum dot. The graph consists of three quasi-1D regions: a central region describing the dot, and two identical left- and right- wires connected to leads, which mimic contacts of a real system. We find the exact solution of the diffusion equation for this graph and evaluate the conductance including quantum corrections. Our model is complementary to the RMT models describing quantum dots. Firstly, it reproduces the universal limit at zero temperature. But the main advantage compared to RMT models is that it allows one to take into account interaction-induced dephasing at finite temperatures. Besides, the crossovers from open to almost closed quantum dots and between different regimes of dephasing can be described within a single framework. We present results for the temperature dependence of the weak localization correction to the conductance for the experimentally relevant parameter range and discuss the possibility to observe the elusive 0D-regime of dephasing in different mesoscopic systems.

1 Introduction

In the last decades, dephasing in quantum dots has been studied experimentally and theoretically in great detail. The theoretical description is largely based on results from random matrix theory (RMT), emphasizing the universality in the description of a dot, when spatial degrees of freedom become negligible. While the universal limits are well understood and reproduced in many experiments, a prediction of the full temperature dependence of quantities which are sensitive to dephasing, such as quantum corrections to the classical conductance, Δg, are challenging existing theories. Since RMT is not able

to describe the T dependence on its own, several extensions were introduced in the past to describe their dependence on a dephasing time τ_φ, which has to be included phenomenologically, see Sect. 2 for details.

One of the well-know problems in the theory of dephasing in quantum dots originated from the predictions of a seminal paper by Sivan, Imry and Aronov, who showed that dephasing in the so-called 0D regime ($T \ll E_{\mathrm{Th}}$, where E_{Th} is the Thouless energy), behaves as $\tau_\varphi \sim T^{-2}$, which results from Pauli blocking of the Fermi sea [1]. However fundamental the origin of 0D dephasing is, it has so far not been observed experimentally. One possible reason for this might be the fact that dephasing is very weak in this regime, such that quantum corrections may reach their universal limit $\Delta g \sim 1$. In general, if the dephasing time is much larger than the time the electron spends in the dot, Δg is governed by a dwelling time τ_{dw} and becomes almost T independent. The remaining small T-dependent part of Δg can be masked, for example, by other T-dependent effects coming from contacts or leads. Thus, to facilitate an experimental observation of 0D dephasing, a comprehensive theory of transport in the quantum dot connected to leads via some contacts is needed, which goes beyond the simple picture provided by RMT.

In this paper we propose an alternative to the RMT description of the quantum dots. Namely, we follow the ideas of [2,3] and model the quantum dot as a network of 1D wires and use the theory of diffusion in graphs to calculate τ_φ and Δg. Earlier papers either focused only on small graphs, such as 1D rings [4–6], or the authors intro-

---

* Corresponding author
  E-mail: Maximilian.Treiber@physik.lmu.de,
  Phone: +49 (0)89 2180 4533
Ludwig Maximilians University, Arnold Sommerfeld Center and Center for Nano-Science, Munich, 80333, Germany

WILEY ONLINE LIBRARY

duced τ_φ only phenomenologically [2, 3, 7]. We generalize the theory of τ_φ for arbitrary graphs and include the regime $T < E_{\mathrm{Th}}$ by taking into account the Pauli principle. Using this theory, we calculate τ_φ for a network describing a quantum dot, taking into account effects of the contacts and the leads. This allows us to demonstrate that the T^2-dependence of the dephasing rate in 0D regime is substantially distorted in usual transport measurements in quantum dots.

The rest of the paper is organized as follows: In Sect. 2 we give a brief review of known results for dephasing in quantum dots. In Sect. 3, basic results from the theory of diffusion in graphs are presented, and in Sect. 4 we will apply this theory to construct a solvable quantum dot model as an alternative to the well-known RMT models. Results for the quantum corrections to the conductance and the dephasing time are presented in the following Sections. In the conclusions we compare different experimental setups where 0D dephasing could be observed.

2 Dephasing in quantum dots: Brief review of known results

It is well-known that the conductance g of a disordered normal metal is reduced due to quantum mechanical interference of the electron wave functions scattered at static impurities. It has been found that the reduction of g can be expressed via the return probability of coherent electron paths, $P(\boldsymbol{x}, \boldsymbol{x}, t)$, (the so-called *Cooperon*) integrated over time and space [8]:

$$\Delta g \equiv g - g_0 = -4 E_{\mathrm{Th}} \int_0^\infty \mathrm{d}t \int \mathrm{d}^d \boldsymbol{x} \, P(\boldsymbol{x}, \boldsymbol{x}, t). \qquad (1)$$

Here g_0 is the classical conductance measured in units of e^2/h, $E_{\mathrm{Th}} = D/\Omega^2$ is the Thouless energy of the system, D is the diffusion constant and Ω is the largest size of the system. Δg is usually referred to as the *weak localization correction*.

Quantum coherence is suppressed by a constant magnetic field and by time-dependent (noisy) fields, or when closed electron paths contributing to $P(\boldsymbol{x}, \boldsymbol{x}, t)$ in Eq. (1) are dephased due to inelastic scattering events. The time-scale associated with the latter is called *dephasing time* τ_φ. In the absence of other sources of dephasing, τ_φ yields an infrared cutoff for the time-integral, Eq. (1), and governs the temperature dependence of Δg [9]. At low temperatures, $T \lesssim 1K$, where phonons are frozen, τ_φ is dominated by electron interactions and depends on the dimensionality d and the geometry of the system. The T-dependence of τ_φ in different regimes is governed by an

interplay of τ_φ with the thermal time $\tau_T = 1/T$ and the Thouless time $\tau_{\mathrm{Th}} = 1/E_{\mathrm{Th}}$, see Table 1 for a summary of known regimes in 1D and 2D [10]. For low temperatures and small system sizes, when E_{Th} is the largest energy scale, dephasing becomes effectively zero-dimensional (0D). Therefore, it must be relevant for transport in metallic (diffusive or chaotic) quantum dots [1].

Table 1 Dephasing rate $1/\tau_\varphi$ as a function of temperature T.

	$\tau_T \ll \tau_\varphi \ll \tau_{\mathrm{Th}}$	$\tau_T \ll \tau_{\mathrm{Th}} \ll \tau_\varphi$	$\tau_{\mathrm{Th}} \ll \tau_T \ll \tau_\varphi$
1D	$\propto T^{2/3}$	$\propto T$	$\propto T^2$
2D	$\propto T$	$\propto T \ln(T)$	$\propto T^2$

Note that 0D dephasing requires confinement of the electron paths during times larger than τ_{Th}, since quantum corrections become T independent for $\tau_\varphi \gg \tau_{\mathrm{Th}}$ in fully open systems. As an example, consider the case of a quasi-1D wire of length L connected to absorbing leads, where Δg reads [11]:

$$\Delta g = -4 \sum_{n=1}^\infty \frac{1}{(\pi n)^2 + \tau_{\mathrm{Th}}/\tau_\varphi} \bigg|_{\tau_\varphi \gg \tau_{\mathrm{Th}}} \simeq -\frac{2}{3}. \qquad (2)$$

Thus, a detailed calculation of Δg including τ_φ requires solving the full diffusion equation of the connected quantum dot, which is hard to achieve analytically for confined systems.

One way to circumvent this problem is to apply random-matrix theory (RMT) to the scattering matrix S, describing transmission and reflection in the sample. In such an RMT model one assumes that the elements of the Hamiltonian H describing the systems are either real (Gaussian orthogonal ensemble, $\beta_{\mathrm{GOE}} = 1$) or complex (Gaussian unitary ensemble, $\beta_{\mathrm{GUE}} = 2$) random numbers corresponding to a system with time-reversal symmetry or broken time-reversal symmetry.[1] Imposing a Gaussian probability distribution $P(H)$, the scattering matrix S can be constructed using so-called R-matrix theory. Alternatively, a simpler approach starts from a probability distribution of the scattering matrix directly, which is of the form $P(S) = \mathrm{const}$, and S is again only restricted by symmetry arguments. From the scattering matrix, the full non-pertubative distribution of the transmission matrix

---

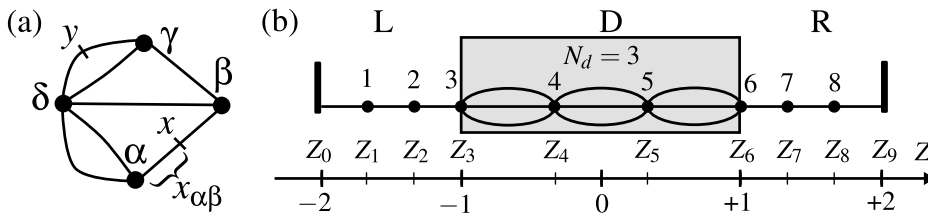[1] Note that in this paper, we consider only the spinless cases.

Figure 1 (a) A graph consisting of 9 wires and 6 vertices, denoted by Greek letters. (b) A quantum dot realized as a graph with dimensionless coordinate $Z = x/L$. The labels Z_i denote the position of the leads ($i = 0, 9$) and the vertices ($i = 1 \ldots 8$) on the scale Z. Furthermore, the numbers $i = 1 \ldots 8$ correspond to the ith row or column of the vertex matrix $\mathcal{M}^\gamma$, Eq. (10)

and the conductance can be obtained. While RMT is unable to predict the temperature dependence of Δg on its own, the difference in g of the cases β_{GOE} and β_{GUE} is equivalent to Δg in the universal limit of $T \to 0$. The universal values for Δg calculated by RMT are ~ 1, in particular $\Delta g = 1/3$ for a quantum dot with spinfull single-channel ($N = 1$) contacts and $\Delta g = 1/4$ for many-channel ($N \to \infty$) contacts [12,13], but we would like to stress that taking into account dimensionality and geometry of the contacts may lead to different values. Extensions to RMT have been introduced in the past to describe the dependence of Δg on a dephasing time [14], e.g. by including a fictitious voltage probe into the scattering matrix which removes electrons from the phase-coherent motion of the electrons in the quantum dot [15], or by including an imaginary potential equal to $-i/2\tau_\varphi$ in the Hamiltonian from which the scattering matrix is derived [16]. It is expected that τ_φ included in such an approach has the same form as stated in Table 1 for $T \ll E_{\text{Th}}$, i.e. $\tau_\varphi \propto T^{-2}$, but a proof of this expectation and a theory of a crossover between different regimes is still missing.

3 Diffusion in graphs

In this section, we present basic results from the theory of diffusion in graphs, following [11]. A graph is defined as a set of quasi-1D wires connected to each other at vertices, see the example shown in Fig. 1(a). In this section we will show how the solution to the Laplace transformed diffusion equation,

$$(\gamma - D\Delta) P_\gamma(x, y) = \delta(x - y),\qquad(3)$$

between arbitrary vertices (with coordinates x and y) of such a graph can be obtained. The time-dependent probability, required to calculate Δg and τ_φ, can be obtained via an inverse Laplace transform:

$$P(x, y, t) = \frac{1}{2\pi i} \int_{-i\infty}^{+i\infty} d\gamma \, e^{\gamma t} P_\gamma(x, y).\qquad(4)$$

It is convenient to introduce the following quantities: We denote the wire between arbitrary vertices α and β as $(\alpha\beta)$ and its length as $L_{\alpha\beta}$. Furthermore, *the running coordinate* along this wire (measured from α) is denoted $x_{\alpha\beta}$, and in the following, we will not distinguish a vertex from the coordinate of the vertex on the graph: For example, $P(\alpha, y)$ is equivalent to $\lim_{x_{\alpha\beta} \to 0} P(x_{\alpha\beta}, y)$, for any neighboring vertex β of α. The current conservation at some vertex α can be written as follows:

$$-\overline{\sum_{(\alpha\beta)}} \left[\partial_{x_{\alpha\beta}} P_\gamma(\mu, x_{\alpha\beta}) \right]_{x_{\alpha\beta}=0} = \delta_{\alpha,\mu},\qquad(5)$$

where the symbol $\overline{\sum}_{(\alpha\beta)}$ means summation over all wires $(\alpha\beta)$ which are connected to α.

Consider the point x lying at the coordinate $x_{\alpha\beta}$ of wire $(\alpha\beta)$ in Fig. 1(a). The probability to reach x from some arbitrary other point y of the graph can be expressed in terms of the probabilities from the neighboring vertices of x, i.e. α and β:

$$P_\gamma(y, x) = \qquad(6)$$

$$\frac{P_\gamma(y, \alpha) \sinh\left(\sqrt{\gamma/D}\,(L_{\alpha\beta} - x_{\alpha\beta})\right) + P_\gamma(y, \beta) \sinh\left(\sqrt{\gamma/D}\,x_{\alpha\beta}\right)}{\sinh\left(\sqrt{\gamma/D}\,L_{\alpha\beta}\right)}.$$

Validity of the solution (6) can be checked directly by substituting Eq. (6) into Eq. (3).

Inserting (6) into (5) yields the following equations for vertex α:

$$P_\gamma(\mu, \alpha) \overline{\sum_{(\alpha\beta)}} \sqrt{\gamma/D} \coth\left(\sqrt{\gamma/D} L_{\alpha\beta}\right)$$

$$- \overline{\sum_{(\alpha\beta)}} P_\gamma(\mu, \beta) \frac{\sqrt{\gamma/D}}{\sinh\left(\sqrt{\gamma/D}L_{\alpha\beta}\right)} = D\delta_{\alpha,\mu}.\qquad(7)$$

Writing down Eq. (7), for every vertex of the graph, we obtain a set of linear equations which can be solved for ar-

bitrary vertices. Let us define a matrix $\mathcal{M}^\gamma$ as follows:

$$
\mathcal{M}^\gamma_{\alpha\beta} \equiv \overline{\sum_{(\alpha\delta)}} \left(\delta_{\alpha\beta} \sqrt{\gamma/D} \coth\left(\sqrt{\gamma/D} L_{\alpha\delta}\right) \right.
$$
$$
\left. -\delta_{\delta\beta} \sqrt{\gamma/D} \sinh\left(\sqrt{\gamma/D} L_{\alpha\delta}\right)^{-1} \right). \tag{8}
$$

It is easy to check that the diffusion probability between arbitrary vertices of the graph is given by the entries of the inverse matrix divided by the diffusion constant [7, 11]:

$$
P_\gamma(\alpha,\beta) = \frac{1}{D} (\mathcal{M}^\gamma)^{-1}_{\alpha\beta}. \tag{9}
$$

4 A graph model for a connected quantum dot

In this section we explain how to describe a connected quantum dot by a network of 1D wires. The main advantage of this model is that an exact solution to the diffusion equation can be found.

Consider the network shown in Fig. 1(b). It includes 8 vertices and describes a quantum dot of total length $2L$ attached via two contacts of length L to absorbing leads.[2] Multiple wires connecting the same vertices (e.g. the three wires connecting vertex 4 with vertex 5) mimic a larger number of channels. Below, we use a dimensionless coordinate $Z = x/L$; the position of the leads is fixed at $Z_0 = -2$, $Z_9 = +2$ and the position of the 3rd and

running coordinates can be expressed via the length of the connecting wires, e.g. the length of the wire connecting vertices 1 and 2 is given by $(Z_2 - Z_1)$.

To describe confinement of the electrons, we assume that all vertices in the regions L and R (including boundaries) are connected by single wires while the vertices in the dot (including its boundaries) are connected via N_d wires. This allows us to tune the system from a simple wire at $N_d = 1$ to an almost closed quantum dot for $N_d \to \infty$. The corresponding vertex matrix $\mathcal{M}^\gamma$, defined in Eqs. (8), is given by

$$
\mathcal{M}^\gamma =
\begin{pmatrix}
[\mathcal{M}^\gamma_L] & 0 & 0 & 0 & 0 & 0 & 0 \\
& S_L & 0 & 0 & 0 & 0 & 0 \\
0 & S_L & C_{LD} & S_{LD} & 0 & 0 & 0 \\
0 & 0 & S_{LD} & [\mathcal{M}^\gamma_D] & 0 & 0 & 0 \\
0 & 0 & 0 & & S_{DR} & 0 & 0 \\
0 & 0 & 0 & 0 & S_{DR} & C_{DR} & S_R & 0 \\
0 & 0 & 0 & 0 & 0 & S_R & [\mathcal{M}^\gamma_R] \\
0 & 0 & 0 & 0 & 0 & 0 &
\end{pmatrix}. \tag{10}
$$

We have introduced 2×2 blocks,

$$
\mathcal{M}^\gamma_L = \mathcal{M}^\gamma_{0123}, \qquad \mathcal{M}^\gamma_D = N_d \mathcal{M}^\gamma_{3456}, \qquad \text{and}
$$
$$
\mathcal{M}^\gamma_R = \mathcal{M}^\gamma_{6789}, \tag{11}
$$

which are given by:

$$
\mathcal{M}^\gamma_{ijkl} =
\begin{pmatrix}
\coth\left(\sqrt{\tilde\gamma}[Z_j - Z_i]\right) + \coth\left(\sqrt{\tilde\gamma}[Z_k - Z_j]\right) & -1/\sinh\left(\sqrt{\tilde\gamma}[Z_k - Z_j]\right) \\
-1/\sinh\left(\sqrt{\tilde\gamma}[Z_k - Z_j]\right) & \coth\left(\sqrt{\tilde\gamma}[Z_k - Z_j]\right) + \coth\left(\sqrt{\tilde\gamma}[Z_l - Z_k]\right)
\end{pmatrix}. \tag{12}
$$

6th vertex, describing the connection of the dot to the contacts, is fixed at $Z_3 = -1$, $Z_6 = +1$. The remaining 6 vertices are auxiliary: There are 3 regions in the system marked by "L" (left contact), "D" (dot) and "R" (right contact). We would like to describe diffusion from an arbitrary point in the system to another. Therefore, we have to place two additional vertices in each region L, D, R. Positions of these vertices define running coordinates. They are arbitrary within the corresponding region, thus each region is subdivided into 3 wires of varying length. The

Expressions for the entries "S" and "C", which correspond to connected vertices, read

$$
S_{L;R} = -1/\sinh\left(\sqrt{\tilde\gamma}(-1 \mp Z_{2;7})\right),
$$
$$
S_{LD;DR} = -N_d/\sinh\left(\sqrt{\tilde\gamma}(1 \pm Z_{4;5})\right),
$$
$$
C_{LD;DR} = N_d \coth\left(\sqrt{\tilde\gamma}(1 \pm Z_{4;5})\right) + \coth\left(\sqrt{\tilde\gamma}(-1 \mp Z_{2;7})\right),
$$

where we have defined the dimensionless parameter $\tilde\gamma = \gamma/E_{\mathrm{Th}}$, where $E_{\mathrm{Th}} = D/L^2$ is the Thouless energy on the scale L. Note that the total length of the wires which form the graph is $L_{\mathrm{total}} = 2L(N_d + 1)$. Thus, the probabilities obtained via inversion of the matrix (10), cf. Eq. (9), are normalized on L_{total}. For further calculations, it is more convenient to change this normalization from L_{total} to the actual length of the system, $4L$: Firstly, we recall that all N_d wires in the dot connecting the same two vertices have the same length, i.e. these wires are identical. Consider a

---

[2] We have chosen this particular ratio of wire lengths to simplify the calculations in the remainder of this section. Note that neither very short nor very long connecting wires are experimentally relevant for quantum dots, since either the confinement to the central region would be lost or the contacts would be unrealistically large.
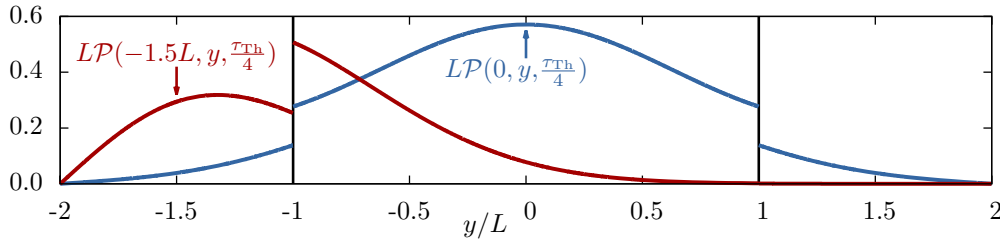
Figure 2 (online color at: www.ann-phys.org) Probability as a function of space for fixed $t = \tau_{\text{Th}}/4$, $N_d = 2$ and initial position $x = -1.5L$ (red curve) or $x = 0$ (blue curve). The initial positions are marked by arrows.

point $\mathcal{X}$ inside the dot which belongs a given wire (out of N_d) and is infinitesimally close to one of the vertices $\alpha = 4$ or 5. The probability to reach $\mathcal{X}$ from any other point is equal to the probability to reach α itself. Let us now introduce a probability $\mathcal{P}$ to reach $\mathcal{X}$ belonging to *any* of the N_d wires:

$$\mathcal{P}_\gamma(\alpha, \beta) = N^{(\beta)} P_\gamma(\alpha, \beta) \equiv N^{(\beta)} \frac{1}{D} (\mathcal{M}^\gamma)^{-1}_{\alpha\beta}; \tag{13}$$

here $N^{(\beta)} = N_d$ if β is a vertex lying in the dot and $N^{(\beta)} = 1$ otherwise. $\mathcal{P}$ is normalized on $4L$ and it reflects an enhancement of the probability for an electron to stay in the dot by the factor N_d.

Furthermore, we define the *piecewise continuous* function $\mathcal{P}_\gamma(x, y)$ of *continuous* variables $x, y \in [-2L, 2L]$ by selecting two appropriate vertices and replacing the wire-length parameters, Z_α, by x/L or y/L. For example, the probability to reach any point $y \in [-L, L]$ in the dot from a point $x \in [-2L, -L]$ in the left contact, is given by $\mathcal{P}_\gamma(x, y) = N_d \frac{1}{D} (\mathcal{M}^\gamma)^{-1}_{14}$ after replacing Z_1 by x/L and Z_4 by y/L.

An analytic expression for $\mathcal{P}_\gamma(x, y)$ can be evaluated efficiently, but it is lengthy and will be published elsewhere. Besides, the inverse Laplace transform of $\mathcal{P}_\gamma(x, y)$, cf. Eq. (4), can be calculated by exploiting the fact that all poles of $\mathcal{P}_\gamma(x, y)$ are simple and coincide with the zeros of the determinant of $\mathcal{M}^\gamma$. Direct calculation yields[3]

$$\det \mathcal{M}^\gamma \propto S(\tilde{\gamma})$$

$$\equiv \sinh\left(2\sqrt{\tilde{\gamma}}\right)\left((N_d - 1) + (N_d + 1)\cosh\left(2\sqrt{\tilde{\gamma}}\right)\right). \tag{14}$$

---

[3] We note in passing that $S(\tilde{\gamma})$ is proportional to the so-called spectral determinant, $\det(-D\Delta + \gamma)$, of the graph [11], implying that it does not depend on any of the auxiliary coordinates Z_i.

Solving equation $S(\tilde{\gamma}) = 0$ yields the following poles for the graph under consideration:

$$\tilde{\gamma}_k = -\left(\frac{k\pi}{2}\right)^2, \quad k \in \mathbb{N}^+, \quad \text{or}$$

$$\tilde{\gamma}_k = -\left(k\pi + \arccos\sqrt{\frac{N_d}{N_d + 1}}\right)^2, k \in \mathbb{Z}. \tag{15}$$

Note that there is no pole at $\tilde{\gamma} = 0$ since the system is open. Defining the dimensionless function

$$\mathcal{R}(x, y, \tilde{\gamma}) = \frac{D}{L} \frac{\mathcal{P}_{\tilde{\gamma}E_{\text{Th}}}(x, y) S(\tilde{\gamma})}{S'(\tilde{\gamma})}, \tag{16}$$

where $S'(x) = \partial_x S(x)$, we can evaluate the time-dependent probability using the residue theorem by closing the integral contour in Eq. (4) on the left half-plane:

$$\mathcal{P}(x, y, t) = \frac{1}{L} \sum_k \mathcal{R}(x, y, \tilde{\gamma}_k) \exp\left(\tilde{\gamma}_k E_{\text{Th}} t\right). \tag{17}$$

$\mathcal{P}(x, y, t)$ is plotted in Fig. 2 for fixed $t = \tau_{\text{Th}}/4$, $N_d = 2$ and x either in the left contact or in the dot. We emphasize that for $N_d > 1$, $\mathcal{P}(x, y, t)$ is discontinuous at $y = \pm L$, describing confinement in the dot. In particular, $\mathcal{P}(x, y, t) = N_d \mathcal{P}(y, x, t)$ for x in a contact and y in the dot. Normalization is reflected by the fact that $\mathcal{P}(x, y, t)$ satisfies a semi-group relation

$$\int_{-2L}^{2L} dy \mathcal{P}(x, y, t_1) \mathcal{P}(y, z, t_2) = \mathcal{P}(x, z, t_1 + t_2). \tag{18}$$

In the next sections we will evaluate the correction to the conductance and the dephasing time using the probability $\mathcal{P}$.

5 Quantum corrections to the conductance for the quantum dot model

The classical conductance of the system described by Eq. (10) is obtained via Kirchhoff's circuit laws, since the contacts of length L and the central region of length $2L$

(with N_d wires in parallel) are connected in series. Denoting the contact conductance (i.e. the conductance of the left or right wire) as g_c, we obtain

$$g_0 = \frac{g_c}{2}(1 + 1/N_d)^{-1}. \qquad (19)$$

Note that the value of g_c cannot be chosen arbitrarily: Assuming that the substrate, from which the wire (length L and width W) is constructed, is 2D or 3D with mean free path ℓ and Fermi wavelength λ_F, the conductance is given by $g_c^{2D} = \ell W / \lambda_F L$ or $g_c^{3D} = 2\ell W^2 / 3\pi \lambda_F^2 L$. Our theory requires $g_c > 4/3$ in order to obtain $g > \Delta g$, and quasi-1D diffusion requires $\lambda_F \ll \ell, W \ll L$. For a quantum-dot of the size of several μm, etched on a GaAs/AlGaAs heterostructure ($\lambda_F \approx 0.05$ μm), we can estimate a typical value of $g_c \sim 5$.

To evaluate the quantum corrections Δg, Eq. (1), we need the return probability defined via Eq. (13) at coinciding α and β. In this section, we consider the case $T = 0$ (i.e., $\tau_\varphi \to \infty$) and study Δg as a function of the dissipation parameter γ. We calculate matrix elements $[(\mathcal{M}^\gamma)^{-1}]_{11}$, $[(\mathcal{M}^\gamma)^{-1}]_{44}$ which yield the return probability for the dot:

$$\mathcal{P}_\gamma(x,x)\Big|_{x\in[-L,L]} = \frac{1}{2\sqrt{\gamma D}(N_d+1)S(\tilde{\gamma})}$$

$$\times \left[(N_d-1)\sinh\left(\sqrt{\tilde{\gamma}}\frac{x}{L}\right) - (N_d+1)\sinh\left(\sqrt{\tilde{\gamma}}\left(\frac{x}{L}-2\right)\right) \right]$$

$$\times \left[(N_d+1)\sinh\left(\sqrt{\tilde{\gamma}}\left(\frac{x}{L}+2\right)\right) - (N_d-1)\sinh\left(\sqrt{\tilde{\gamma}}\frac{x}{L}\right) \right]; \quad (20)$$

and for the left wire:

$$\mathcal{P}_\gamma(x,x)\Big|_{x\in[-2L,-L]} = \frac{\sinh\left(\sqrt{\tilde{\gamma}}(\frac{x}{L}+2)\right)}{2\sqrt{\gamma D}(N_d+1)S(\tilde{\gamma})} \qquad (21)$$

$$\times \Big[(N_d-1)\Big((N_d+1)\sinh\left(\sqrt{\tilde{\gamma}}\frac{x}{L}\right) + (N_d-1)\sinh\left(\sqrt{\tilde{\gamma}}\left(\frac{x}{L}+2\right)\right)$$

$$- (N_d+1)\sinh\left(\sqrt{\tilde{\gamma}}\left(\frac{x}{L}+4\right)\right)\Big) - (N_d+1)^2\sinh\left(\sqrt{\tilde{\gamma}}\left(\frac{x}{L}-2\right)\right) \Big];$$

respectively. $\mathcal{P}_\gamma(x,x)$ for the right wire, $x \in [L, 2L]$, can be obtained from the symmetry property $\mathcal{P}_\gamma(x,x) = \mathcal{P}_\gamma(-x,-x)$. In the limit $\gamma \to 0$, Eqs. (20) and (21) reduce to

$$\mathcal{P}_0(x,x)\Big|_{x\in[-L,L]} = \frac{L((N_d+1)^2 - (\frac{x}{L})^2)}{2D(N_d+1)},$$

$$\mathcal{P}_0(x,x)\Big|_{x\in[-2L,-L]} = \frac{L(2+\frac{x}{L})(2-N_d\frac{x}{L})}{2D(N_d+1)}. \qquad (22)$$

Note that the return probability diverges for $x \in [-L, L]$ in the limit $N_d \to \infty$, since the central region is effectively closed in this limit.

Similarly to Eq. (19), the total quantum corrections have to be properly weighted by using the circuit laws. The total correction can be written as a sum over all wires i of the network [17]:

$$\Delta g = -4D\frac{1}{\mathcal{L}^2}\sum_i \frac{\partial \mathcal{L}}{\partial L_i}\int_{\text{Wire No. }i} \mathrm{d}x \mathcal{P}_\gamma(x,x), \qquad (23)$$

where $\mathcal{L}$ is the effective total length of the system obtained similar to the total resistance. In the case under consideration, we have

$$\mathcal{L} = L_0 + \frac{1}{1/L_1 + \cdots + 1/L_{N_d}} + L_{N_d+1} = 2L(1+1/N_d), \qquad (24)$$

where $L_0 = L$ corresponds to the left wire, $L_{N_d+1} = L$ to the right wire and $L_1 \ldots L_{N_d} = 2L$ to the N_d wires of the dot. We obtain the following expression for the total quantum correction:

$$\Delta g = -E_{\text{Th}}\frac{1}{(1+1/N_d)^2}\left[\int_{-2L}^{-L}\mathrm{d}x\, \mathcal{P}_\gamma(x,x) \right.$$

$$\left. + \frac{1}{N_d^2}\int_{-L}^{L}\mathrm{d}x\, \mathcal{P}_\gamma(x,x) + \int_{L}^{2L}\mathrm{d}x\, \mathcal{P}_\gamma(x,x) \right]. \qquad (25)$$

In Fig. 3, we show the total correction to the conductance according to Eq. (25) as a function of the dissipation parameter γ for different values of N_d. Note that for

$\Delta g = 2/3$

$\Delta g = 1/3$

$\propto 1/\sqrt{\tilde{\gamma}}$

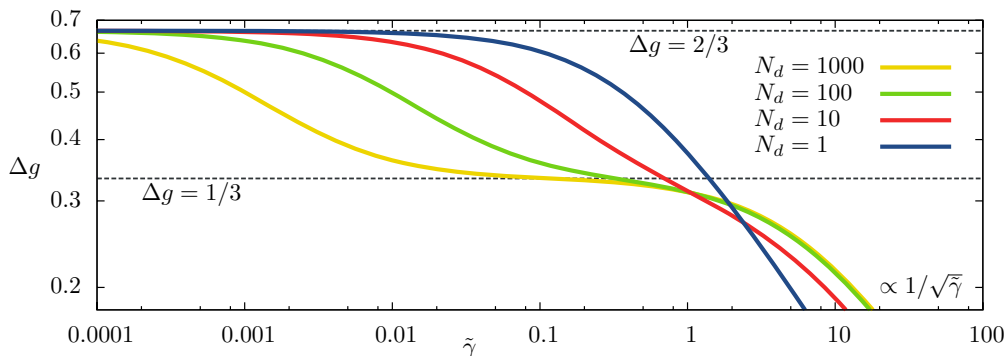|	
$N_d = 1000$	
$N_d = 100$	
$N_d = 10$	
$N_d = 1$	

Figure 3 (online color at: www.ann-phys.org) Dependence of the total quantum correction to the conductance of the quantum dot model, Eq. (25), on the dimensionless dissipation parameter $\tilde{\gamma} = \gamma/E_{\text{Th}}$.

$\gamma \gg 1$ all curves are $\propto 1/\sqrt{\gamma}$, similar to an infinite wire with different prefactors corresponding to different effective wire width. We are mainly interested in the regime $\gamma \ll 1$, where the main result originates from the left and right wire and all curves approach the ergodic limit $\lim_{\gamma \to 0}(\Delta g) = 2/3$, cf. Eq. (2). This limit can be checked in this model by substituting Eqs. (22) into Eq. (25). Thus, in the absence of dissipation, our model has qualitatively the same behavior as RMT theory, albeit the precise universal value differs by a factor ~ 1, cf. Sect. 2. This difference is due to the fact that RMT assumes structureless contacts and is a 0D model, whereas the validity of the graph model requires $L \gg (W, \ell)$ for the connecting quasi-1D wires. Since the time to reach one contact from the other increases linearly with N_d, there is an intermediate regime at $1/N_d < \tilde{\gamma} < 1$ for large N_d, where the system is described effectively as two wires connected in series via the dot, which just plays the role of an additional lead, such that $\Delta g = 1/3$.

6 Evaluation of the dephasing time for the quantum dot model

The dephasing time, τ_φ, can be calculated from the phase difference acquired by an electron in a time-dependent (fluctuating) potential $V(x,t)$ during a time-reversed traversal of its trajectory $x(t)$ [9]:

$$\Phi[x(\tau)] = \int_0^t d\tau \left[V(x(\tau), \tau) - V(x(\tau), t - \tau) \right]. \tag{26}$$

When averaged over the Gaussian fluctuations of the potential $\langle e^{i\Phi} \rangle_V = e^{-\frac{1}{2}\langle \Phi^2 \rangle V}$, Eq. (26) leads to an exponential cutoff of the return probability[4]

$$\mathcal{P}(x,x,t) \to \mathcal{P}(x,x,t) \cdot \langle e^{i\Phi[x(\tau)]} \rangle_{\{x(\tau)\}} \approx \mathcal{P}(x,x,t) \cdot e^{-\mathcal{F}(x,t)} \tag{27}$$

where $\langle \dots \rangle_{\{x(\tau)\}}$ means the average is over closed trajectories $x(\tau)$ of duration t, staring and ending at x, and we defined the decay function $\mathcal{F}$ [18, 19]:

$$\mathcal{F}(x,t) = \int_0^t dt_{1,2} \langle \langle VV \rangle (x(t_1), x(t_2), t_1 - t_2)$$

$$- \langle VV \rangle (x(t_1), x(t_2), t - t_1 - t_2) \rangle_{\{x(\tau)\}}. \tag{28}$$

---

[4] Note that in the second equality of Eq. (27), we exponentiate the average over closed path, see [18] for details.

In the case of the graph model for the quantum dot, the usual operational definition of τ_φ reads

$$\mathcal{F}(x, \tau_\varphi(x)) = 1, \tag{29}$$

such that the correction to the conductance is given by Eq. (25) with a position dependent $\gamma(x) = 1/\tau_\varphi(x)$. The correlation function $\langle VV \rangle$ entering Eq. (28) is well known for the case of electron interactions in macroscopically homogeneous disordered systems [9]. Recently, we have generalized this theory for inhomogeneous, multiply-connected systems [10]. It has been shown that $\langle VV \rangle$ generically is given by

$$\langle VV \rangle (x, y, t) = \frac{4\pi T}{g_c L} P_0(x, y) \delta_T(t), \tag{30}$$

where $P_0(x, x) = \lim_{\gamma \to 0} P_\gamma(x, x)$ and

$$\delta_T(t) = \pi T w(\pi T t) \quad \text{with} \quad w(x) = \frac{x \coth(x) - 1}{\sinh^2 x} \tag{31}$$

is a broadened δ-function which allows us to take into account the Pauli principle [18].

Inserting Eq. (30) into Eq. (28), we find

$$\mathcal{F}(x,t) = \frac{4\pi T}{g_c} \int_0^t dt_{1,2} \, Q(x, t_m, t_M - t_m, t - t_M)$$

$$\times \left[\delta_T(t_1 - t_2) - \delta_T(t_1 + t_2 - t) \right], \tag{32}$$

where $t_m = \min[t_1, t_2]$ and $t_M = \max[t_1, t_2]$. The function Q is given by the dimensionless quantity $D P_0 / L$, averaged over closed random walks:

$$Q(x_0, t_1, t_2, t_3) = \int_{-2L}^{2L} dx_{1,2}$$

$$\times \frac{\mathcal{P}(x_0, x_1, t_1)\mathcal{P}(x_1, x_2, t_2)\mathcal{P}(x_2, x_0, t_3)}{\mathcal{P}(x_0, x_0, t_1 + t_2 + t_3)} \frac{D P_0(x_1, x_2)}{L}. \tag{33}$$

All probabilities in Eq. (33) can be evaluated analytically from Eq. (17), Eq. (13) and Eq. (10), by deriving the corresponding entries in the inverted vertex matrix $[\mathcal{M}^\gamma]^{-1}$. The integrand is lengthy and we have chosen the following strategy for calculating the integrals:

1) We use Eq. (17) to rewrite Eq. (33) as:

$$Q(x_0, t_1, t_2, t_3)$$

$$= \sum_{n,k,l} \frac{\mathcal{Q}(x_0, \tilde{\gamma}_n, \tilde{\gamma}_k, \tilde{\gamma}_l)}{\mathcal{P}(x_0, x_0, t_1 + t_2 + t_3)} e^{\tilde{\gamma}_n t_1 + \tilde{\gamma}_k t_2 + \tilde{\gamma}_l t_3}, \text{ with} \tag{34}$$

$$\mathcal{Q}(x_0, \tilde{\gamma}_1, \tilde{\gamma}_2, \tilde{\gamma}_3) = D \int \frac{dx_{1,2}}{L^3}$$

$$\times \mathcal{R}(x_0, x_1, \tilde{\gamma}_1)\mathcal{R}(x_1, x_2, \tilde{\gamma}_2)\mathcal{R}(x_2, x_0, \tilde{\gamma}_3) P_0(x_1, x_2). \tag{35}$$

Ann. Phys. (Berlin) 524, No. 3–4 (2012)

annalen der **physik**

Original Paper

The integrals in Eq. (35) over space are evaluated symbolically with the help of a computer algebra program.

2) Since the time dependence of Q in Eq. (34) is simply exponential, one of the time-integrals in Eq. (28) is calculated analytically. As a result, $F(x_0, t)$ simplifies to a single time integral and multiple sums:

$$F(x_0, t)$$

$$= \frac{(4\pi)^2}{g_c} \frac{\sum_{n,k,l} \mathcal{Q}(x_0, \tilde{\gamma}_n, \tilde{\gamma}_k, \tilde{\gamma}_l) \int_0^{tT} d\tau \, \mathcal{E}(\tau, \tilde{\gamma}_n, \tilde{\gamma}_k, \tilde{\gamma}_l)}{\sum_m \mathcal{R}(x_0, x_0, \tilde{\gamma}_m) e^{\tilde{\gamma}_m E_{\mathrm{Th}} t}}. \quad (36)$$

Here, the remaining time dependence of the kernel is incorporated in the function $\mathcal{E}$:

$$\mathcal{E}(\tau, \tilde{\gamma}_1, \tilde{\gamma}_2, \tilde{\gamma}_3) = w(\pi\tau) e^{c_1 tT}$$

$$\times \left[\frac{\sinh(c_2(tT-\tau)) e^{c_3\tau}}{2c_2} \right.$$

$$\left. - \frac{\sinh\left(\frac{c_3}{2}(tT-\tau)\right) \cosh(c_2\tau) e^{c_3(tT-\tau)/2}}{c_3} \right], \quad (37)$$

with

$$c_1 = (\tilde{\gamma}_1 + \tilde{\gamma}_3)\frac{E_{\mathrm{Th}}}{2T}, \quad c_2 = (\tilde{\gamma}_1 - \tilde{\gamma}_3)\frac{E_{\mathrm{Th}}}{2T},$$

$$c_3 = \tilde{\gamma}_2 \frac{E_{\mathrm{Th}}}{T} - c_1. \quad (38)$$

3) The sums and the integral over τ are calculated numerically.

This strategy allows us to calculate τ_φ and to describe the T-dependence of Δg in the quantum dot model, including the full crossover between different regimes of dephasing.

7 Examples of application

In this section, we use the graph model of the quantum dot to calculate $\tau_\varphi(x_0, T)$ and $\Delta g(T)$ in the case $g_c = 5$ for the parameter N_d ranging from $N_d = 1$ (no confinement in the central region) to $N_d = 100$ (almost closed quantum dot connected to ideal leads via two contacts). Our model is valid for this choice of g_c, see the discussion in Sect. 5, and the total conductance of the system $1.25 < g_0 < 2.5$ is close to experimental setups [20, 21]. The results are shown in Fig. 4.

The dephasing time is shown in Fig. 4(a) for several values of the origin of the Cooperon, x_0, which can belong either to the central region (solid blue lines) or the contact (dashed red lines). To check the validity of the results, we compare τ_φ at high and small temperatures with earlier results for an almost isolated quasi-1D ring of total length $4L$ and total conductance g_1 [22].

If $\tau_T \ll \tau_\varphi \ll \tau_{\mathrm{Th}} \equiv 1/E_{\mathrm{Th}}$, dephasing is not sensitive to the boundary conditions and it is described by the theory of infinite systems [9]. In the ring, the high-T regime appears at $T \gg g_1 E_{\mathrm{Th}}$. The formula for τ_φ in this regime, including sub-leading terms, reads [22]:

$$\frac{\tau_\varphi}{\tau_{\mathrm{Th}}} = \left(\frac{2g_1 E_{\mathrm{Th}}}{\pi^{3/2} T}\right)^{\frac{2}{3}} \left(1 + \frac{2^{\frac{5}{2}}}{3\pi} |\zeta(1/2)| \left(\frac{\pi^{\frac{3}{2}}}{2g_1}\right)^{\frac{1}{3}} \left(\frac{E_{\mathrm{Th}}}{T}\right)^{\frac{1}{6}} \right.$$

$$\left. + \frac{2}{9\sqrt{\pi}} \left(\frac{2g_1}{\pi^{\frac{3}{2}}}\right)^{\frac{1}{3}} \left(\frac{E_{\mathrm{Th}}}{T}\right)^{\frac{1}{3}}\right). \quad (39)$$

We have reproduced this high-T behavior in the quantum dot model, see Fig. 4(a): Numerically obtained curves coincide with Eq. (39), after substituting $N_d g_c$ for g_1, when $T \gg (g_c N_d) E_{\mathrm{Th}}$. We note that dephasing in the high-T regime is substantially inhomogeneous in space, since the relevant trajectories are restricted to a small region around x_0. In particular, for sufficiently high T, all curves for dephasing in the contact ($N_d = 1, 10, 100$) coincide with the curve for $N_d = 1$ in the central region, since the number of channels in the central region is irrelevant for dephasing in the contact. On the other hand, dephasing in the central region itself becomes weaker with increasing N_d, since N_d increases the effective conductance in this region.

In the low-T regime,[5] $\tau_{\mathrm{Th}} \ll \tau_T \ll \tau_\varphi$, typical electron trajectories explore the whole system many times before dephasing becomes effective [1]. The geometry of the system is not important in this case and, therefore, the low-T regime is usually referred to as *the regime of 0D dephasing*. In the ring, it occurs at $T \ll E_{\mathrm{Th}}$ with τ_φ given by [22]

$$\frac{\tau_\varphi}{\tau_{\mathrm{Th}}} = \frac{135 g_1}{32\pi^2} \left(\frac{E_{\mathrm{Th}}}{T}\right)^2 \left(1 + \frac{16\pi}{45 g_1} \frac{T}{E_{\mathrm{Th}}} + \frac{128\pi^2}{105} \left(\frac{T}{E_{\mathrm{Th}}}\right)^2\right). \quad (40)$$

The quantum dot model shows similar behavior at $T \ll E_{\mathrm{Th}}$, after substituting $g_c N_d$ for the ring conductance.

---

[5] The intermediate regime, $\tau_T \ll \tau_{\mathrm{Th}} \ll \tau_\varphi$, characterized by $\tau_\varphi \propto T^{-1}$ is strongly distorted in the quantum dot, since: (a) The conductance g_c is relatively small, reducing the range of validity of this regime, and (b) it occurs when typical electron trajectories are of the order of the system size making τ_φ sensitive to the inhomogeneities of the graph.
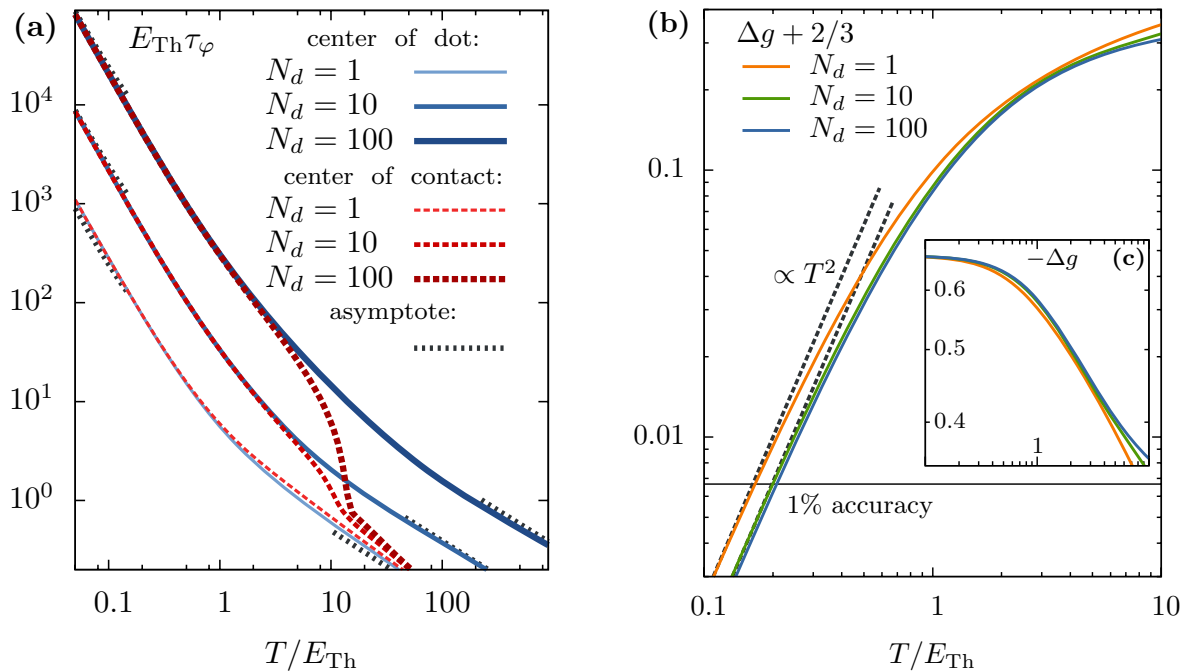
Figure 4 (online color at: www.ann-phys.org) (a) The dephasing time in units of the Thouless time, $1/E_{\mathrm{Th}}$, plotted for several values of N_d and x_0. Solid blue lines, correspond to $x_0 = -0.05L$ close to the center of the dot, while dashed red lines correspond to $x_0 = -1.55L$ close to the center of the left contact. The thickness (and brightness) of the curve determines the number of channels in the dot, $N_d = 1, 10, 100$ from thin to thick (and bright to dark). The black dotted lines correspond to the asymptotic results, Eqs. (39) and (40), derived from an isolated ring geom- etry, see main text for details. (b) The difference $\Delta g + 2/3$ be- tween the correction to the conductance, Δg, and its universal zero-temperature value, $\Delta g(T = 0) = -2/3$, plotted as function of temperature. 0D behavior of the dephasing time, characterized by $\Delta g \propto T^2$, appears at very low temperatures, requiring a preci- sion much larger than 1% on the conductance measurement. In- set: (c) Total correction to the conductance $-\Delta g$ (without subtract- ing $\Delta g(T = 0)$), plotted as function of temperature.

We emphasize that 0D dephasing in our model is gov- erned by atypical trajectories, which explore the dot and the contacts many times during the time scale $t \gg \tau_{\mathrm{dw}}$. Therefore, the dephasing time is nearly coordinate inde- pendent: Dephasing in the central region and in the con- tacts is essentially the same.

The correction to the conductance is shown in the in- set, Fig. 4(c), for $N_d = 1, 10, 100$. We calculated Δg from the integral in Eq. (25) with a position dependent $\gamma(x) = 1/\tau_\varphi(x, T)$. As expected from the discussion in Sect. 5, the curves saturate to the universal value $\Delta g = -2/3$, when $\tilde\gamma \equiv \gamma/E_{\mathrm{Th}} \ll 1/N_d$. Since $1/\tilde\gamma = \tau_\varphi/\tau_{\mathrm{Th}} \sim (g_c N_d)(E_{\mathrm{Th}}/T)^2$ in this regime and g_c is small and fixed, saturation occurs when $T \lesssim E_{\mathrm{Th}}$. The intermediate regime for $1/N_d \ll \tilde\gamma \ll 1$, where $\Delta g = -1/3$, cf. Fig. 3, is strongly distorted since it lies in the crossover region between high-T and low-T regime. We note that at $T < 10 E_{\mathrm{Th}}$, curves for different N_d look very similar. Moreover, dephasing is very weak at $T \ll E_{\mathrm{Th}}$ where Δg is governed by a dwell time, τ_{dw}, of the entire system and is practically T-independent. After subtracting the curve from its universal value, see Fig. 4(b), 0D dephasing reveals itself as $\Delta g \propto T^2$ for very low temperatures $T \lesssim 0.2E_{\mathrm{Th}}$. At $0.2E_{\mathrm{Th}} < T < E_{\mathrm{Th}}$ one can observe only a transient, since (i) dephasing is not yet sufficiently weak to justify $\Delta g \propto T^2$ and (ii) the 0D regime of dephasing is not fully reached, cf. Fig. 4(a). Moreover, if the leads are not perfectly absorbing, the transient can be extended even to lower temperatures due to additional dephasing in the leads. All this clearly shows that 0D dephasing cannot be discovered directly in transport measurements through the quantum dot. Even at $T \lesssim 0.2E_{\mathrm{Th}}$, a fitting of the experimental data would require g to be measured with a precision of much better than 1%. Alternative possibilities for the experi- mental observation of 0D dephasing are discussed in the Conclusions.

Ann. Phys. (Berlin) 524, No. 3–4 (2012)

annalen der **physik**

Original Paper

8 Conclusions

We have suggested a graph model, which allows one to describe transport through mesoscopic quantum dots. The graph includes three quasi-1D regions: identical left- and right- wires and a central region. The identical wires are connected to ideally absorbing leads and mimic the contacts of a real system. The number of conducting channels in the central region can be of the order of- or substantially larger than the number of channels in the contacts. The latter case corresponds to a strong confinement of electrons in the central region. Thus the graph model is able to describe a crossover from opened to closed quantum dots.

The model which we suggest can be viewed as complementary to the seminal RMT model. Firstly, the exact solution to the diffusion equation can be found for the graph model. Secondly, we have shown that our model correctly reproduces the universal regime of transport in full analogy with the RMT solution. Even more importantly, the graph model allows us to take into account interaction induced dephasing in a broad temperature range, i.e., we can describe the full crossover from 1D to 0D regimes.

Using the solution to the diffusion equation on the graph, we have described in detail how to calculate the dephasing time and the weak localization correction to the conductance. Though the intermediate equations are rather lengthy, we have suggested an efficient combination of analytical steps (involving computer algebra) and numerical integration, which helped us to overcome technical difficulties.

The general approach has been illustrated for the system with $g_c = 5$. We have demonstrated that 0D dephasing ($\sim T^2$), which is governed by the Pauli principle and is very generic, occurs in the system at $T \ll E_{\text{Th}}$ at *arbitrary* ratio of the channel numbers in the dots and leads. In this regime, dephasing is governed by atypical trajectories which explore the dot and the contacts many times during the time scale $t \gg \tau_{\text{dw}}$ where the conductance is governed mainly by the dwell time and is almost T-independent. Our results confirm that weak 0D dephasing is substantially distorted by the influence of the contacts and the leads. Therefore, its direct experimental observation in transport through the quantum dot would require not only very low temperatures but also unrealistically precise measurements. We conclude that alternative experimental approaches are needed, where either the effects from the environment are reduced or the system is closed. One possibility to improve the effective precision of the measurements is related to extracting τ_φ from the T-dependence of the Aronov-Altshuler-Spivak oscillations of the magnetoconductivity in almost closed mesoscopic rings. This option was discussed in recent papers [6, 22] where all effects of the environment were taken into account via a constant dwelling time. We plan to study in more detail the sensitivity of the AAS oscillations on the distortions from the environment using a ring model similar to the model of the dot presented here [23]. The other option is to extract τ_φ from experimental measurements of the electric or magnetic susceptibility of *closed* mesoscopic systems, e.g. by measuring the properties of resonators in which mesoscopic samples are deposited [24]. In closed systems, there is no universal limit of the quantum corrections at $\tau_\varphi \gg \tau_{\text{dw}}$, typical for transport through opened systems. Therefore, the saturation in the closed system can occur at much lower T, making them more suitable for an experimental observation of 0D dephasing. A theoretical description of such experiments will be published elsewhere.

References

[1] U. Sivan, Y. Imry, and A. G. Aronov, Europhys. Lett. **28**, 115 (1994).
[2] B. Doucot and R. Rammal, Phys. Rev. Lett. **55**, 1148 (1985).
[3] B. Doucot and R. Rammal, J. Phys. (Paris) **47**, 973 (1986).
[4] T. Ludwig and A. D. Mirlin, Phys. Rev. B **69**, 193306 (2004).
[5] C. Texier and G. Montambaux, Phys. Rev. B **72**, 115327 (2005).
[6] M. Treiber et al., Phys. Rev. B **80**, 201305 (2009).
[7] C. Texier, P. Delplace, and G. Montambaux, Phys. Rev. B **80**, 205413 (2009).
[8] D. E. Khmel'nitskii, Physica B + C **126**, 235 (1984)
[9] B. L. Altshuler, A. G. Aronov, and D. E. Khmelnitsky, J. Phys. C **15**, 7367 (1982).
[10] M. Treiber et al., Phys. Rev. B **84**, 054204 (2011).
[11] E. Akkermans and G. Montambaux, in: Mesoscopic Physics of Electrons and Photons (Cambridge University Press, Cambridge, 2007).
[12] H. U. Baranger and P. A. Mello, Phys. Rev. Lett. **73**, 142 (1994).
[13] R. A. Jalabert, J.-L. Pichard, and C. W. J. Beenakker, Europhys. Lett. **27**, 255 (1994).

Original Paper

[14] P. W. Brouwer and C. W. J. Beenakker, Phys. Rev. B **55**, 4695 (1997).

[15] M. Büttiker, Phys. Rev. B **33**, 3020 (1986).

[16] E. McCann and I. V. Lerner, J. Phys. Condens. Matter **8**, 6719 (1996).

[17] C. Texier and G. Montambaux, Phys. Rev. Lett. **92**, 186801 (2004).

[18] F. Marquardt, J. von Delft, R. Smith, and V. Ambegaokar, Phys. Rev. B **76**, 195331 (2007).

[19] J. von Delft, F. Marquardt, R. Smith, and V. Ambegaokar, Phys. Rev. B **76**, 195332 (2007).

[20] A. G. Huibers et al., Phys. Rev. Lett. **81**, 200 (1998).

[21] S. Amasha et al., arXiv:1009.5348 (unpublished).

[22] M. Treiber et al., Dimensional Crossover of the Dephasing Time in Disordered Mesoscopic Rings: From Diffusive Through Ergodic to 0D Behavior, in: Perspectives of Mesoscopic Physics – Dedicated to Yoseph Imry's 70th Birthday, Chap. 20, edited by A. Aharony and O. Entin-Wohlman (World Scientific, Singapore, 2010); arXiv:1001.0479.

[23] M. Treiber, O. M. Yevtushenko, and J. von Delft, to be published.

[24] R. Deblock et al., Phys. Rev. B **65**, 075301 (2002).